Cost-effective and eco-friendly sprayable nanogels (ZC-CSNG) for multifunctional wound dressing applications

Chemical Engineering Journal 503 (2025) 158312

Contents lists available at ScienceDirect

Chemical Engineering Journal

journal homepage: www.elsevier.com/locate/cej

Cost-effective and eco-friendly sprayable nanogels (ZC-CSNG) for multifunctional wound dressing applications

Suman Basak [a], Priyanka Singh [b], Arjen Weller [c], Firoz Babu Kadumudi [c], Paul J. Kempen [d], Ivan Mijakovic [b,e], Alireza Dolatshahi-Pirouz [c], Kristoffer Almdal [a,*]

[a] Department of Chemistry, Technical University of Denmark, 2800 Kgs. Lyngby, Denmark
[b] The Novo Nordisk Foundation, Center for Biosustainability, Technical University of Denmark, 2800 Lyngby, Denmark
[c] Department of Health Technology, DTU Health Tech, Technical University of Denmark, 2800 Kgs. Lyngby, Denmark
[d] National Centre for Nano Fabrication and Characterization, DTU Nanolab, Technical University of Denmark, 2800 Kgs. Lyngby, Denmark
[e] Systems and Synthetic Biology Division, Department of Biology and Biological Engineering, Chalmers University of Technology, Gothenburg, Sweden

ARTICLE INFO

Keywords:
Sprayable chitosan nanogels
Wound care
ROS therapy
Anti-inflammatory
Antibacterial

ABSTRACT

Chitosan (CS) has significant potential in wound dressing applications, but its utility is limited by poor aqueous solubility. We introduce sprayable nanogels, ZC-CSNG (*zwitterion-modified chitosan-based Schiff base crosslinked nanogels*), which are multifunctional and tailored for biomedical use. These nanogels comprise a 3D network formed by crosslinking chitosan with glutaraldehyde (GA) and incorporating hydrophilic sulfobetaine and antioxidant p-coumaric acid functionalities. Comprehensive characterization confirms the zwitterionic modification of CS and validates the properties of ZC-CSNG. This design improves solubility, protein antifouling efficiency, antibacterial activity, and anti-reactive oxygen species (ROS) properties within a single hydrogel particle system. The green synthesis method, free from organic solvents, ensures solubility, sprayability, and biocompatibility, rendering the ZC-CSNG ideal for wound dressing. Under physiological conditions, these nanogels demonstrate ROS scavenging, stability with a shelf-life exceeding four weeks, and potential to reduce inflammation by scavenging nitric oxide (i.e., NO) *in vitro*. In summary, ZC-CSNG represent a significant advancement in wound dressing technology, offering a promising solution for wound healing. With the capacity to mitigate ROS production, inhibit bacterial growth, reduce inflammation markers, and enhance dermal cellular proliferation, these sprayable nanogels present an efficient wound care option across clinical settings.

1. Introduction

In recent decades, the treatment of local skin wounds has attracted tremendous attention globally [1–2]. For traditional wound dressing, medical gauze and bandage are generally used for wound care therapy [3]. However, hydrogel based systems are of potential interest for wound management due to their excellent biocompatibility and capability to promote wound healing in a moist condition [4–6].

Nano-hydrogels as drug carriers have been extensively investigated over the years utilizing many materials and synthesis techniques, as they are the most versatile nano-carriers, having distinctive capacity of combining the characteristics of 3D matrix materials with the ones of nanoparticles [7–8]. In drug and/or, protein encapsulation [9], nanogels are generally used to reduce the inflammatory response of the organs, to improve bio-distribution [10], further bioavailability and circulation lifetime of the carried drugs [11–12]. Nanogels are soft and moist materials consisting of 3D cross-linked networks *via* covalent or non-covalent bonds, that swell rapidly to equilibrium without dissolution [13–15]. Moreover, nanogels have been extensively investigated in biomedical fields such as biosensing [16], soft-tissue engineering [17], wound-dressing [18], and drug delivery [19] due to their high water retention capacity, excellent cyto-compatibility [20], non-immunogenic and great potential for drug or, small molecules loading [21]. In spite of these advantages most nanogel implants suffer from nonspecific protein binding and immunological response, triggering bacterial adhesion and chronic inflammation [22]. Therefore, it is challenging to develop a new class of materials with the desired antifouling property and high biocompatibility.

Zwitterionic polymers are a new generation of antifouling materials [23]. Zwitterionic materials contain both cationic and anionic groups in

* Corresponding author.
E-mail address: kral@dtu.dk (K. Almdal).

https://doi.org/10.1016/j.cej.2024.158312
Received 18 July 2024; Received in revised form 3 December 2024; Accepted 3 December 2024
Available online 9 December 2024

one functional group while neutrally charged as a whole. The anti-fouling ability of zwitterionic polymers is attributed to the static-induced hydration layer [24]. The unique structure facilitates their increasing applications in biomedical fields. For example, zwitterionic polymer brushes have been demonstrated as promising stealth coatings due to the excellent antifouling performance in human blood [25–26]. Furthermore, zwitterion polymer based drug conjugates can passively kill pathogens [27]. Zwitterions are more stable than polyethylene glycol (PEG) which has common drawbacks like auto degradation of the hydroxyl group to form cell toxic aldehyde, which reduce the antifouling efficacy [28–29].

For these reasons, zwitterion decorated natural polymers has become increasingly interesting for targeted medical treatment of different diseases [30–33]. Two main advantages of using natural polymers are a) easy abundance, eco-friendly and processability; and b) less toxicity of the utilized drug towards the healthy cells. Utilizing such versatile properties, we report a novel class of zwitterion modified chitosan (CS) based biocompatible nanogel systems for wound dressing applications. These nanogels possesses both anti-ROS and antibacterial properties. Antibacterial wound dressings have become increasingly popular in recent years, with most commercial suppliers presently offering silver and other metal coated nanoparticle impregnated dressings [34]. Numerous investigations have additionally documented the significant cytotoxicity of silver nanoparticles towards mammalian cells, as well as their adverse influence on the wound healing process [35]. Moreover, silver dressings for wounds come with a high cost, and persistent worries persist regarding the absorption and potential toxicity of nanoparticles [36]. Consequently, there has been a substantial focus on identifying fresh alternative antimicrobial agents suitable for cellular use. In addition to bacterial concerns, ROS is produced by the wound inflammatory area, which can increase the permeability of the cell capillary wall, leading to damage of vascular endothelial cells and wider cell necrosis and tissue dissolution [37–38]. Although wounds heal gradually over time in moist condition, the presence of external oxidative stimuli and bacterial infections often impedes wound healing process [39]. Antioxidants are expected to block or delay the oxidation process by scavenging free radicals and promote wound recovery [40–41]. Thus, antioxidant therapy could be a promising choice for wound care therapy.

Although several synthetic polymers have been used as drug conjugates, clinical trials did not afford positive effects. CS based materials have attracted increasing research interests because of their lower toxicity, antibacterial nature, and the abundance in nature [42]. The major difficulties with CS particles are to dissolve them in aqueous media due to strong inter-chain attractions. To improve the solubility, we introduce a novel strategy of modifying the CS backbone by sulfobetaine *via* Michael addition. Moreover, a second step modification using p-coumaric acid (p-CA) enhances the anti-ROS and antibacterial effectiveness. p-CA is an excellent scavenger of oxygen free radicals and is thought to be able to diminish the damage caused by oxygen radicals [43]. However, it is difficult to deliver native p-CA under physiological conditions due to its hydrophobicity. It contains a reactive phenolic group for ROS scavenging and the carboxylic acid (–COOH) terminal is used to covalently bind to the CS backbone. These aromatic phenolic moieties not only make p-CA resistant to oxidation but also enable p-CA to be an ultraviolet skin protective agent, as the aromatic moieties allow p-CA acid to absorb UV radiation.

We introduce a novel sprayable nanogel system derived from natural chitosan (CS) polymer derivatives, leveraging its abundant polysaccharide properties for facile synthesis (Fig. 1). We hypothesize for three reasons that the studied materials will outperform traditional wound dressings in promoting wound healing. 1: The sprayable nanogels, which allows versatile wound care management. 2: The enhanced biocompatibility of the zwitterion-modified chitosan nanogels. 3: The

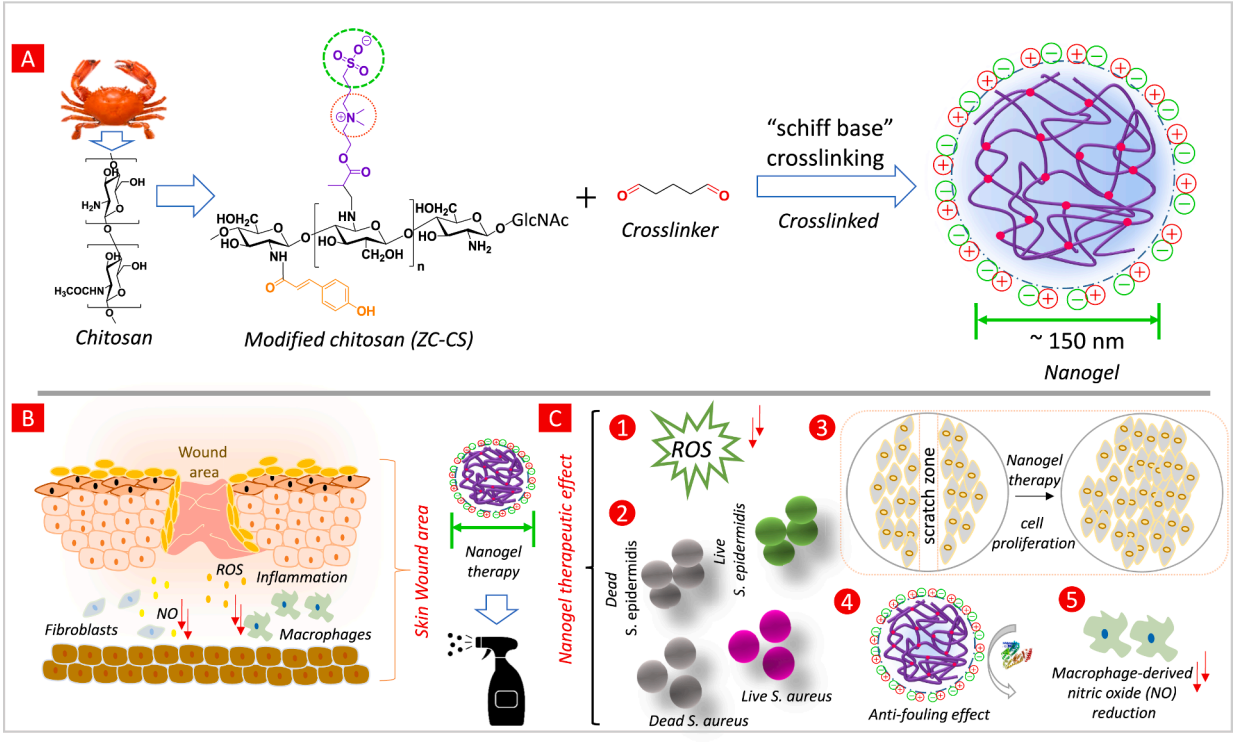

Fig. 1. Overall nanogel design and application to the wound care therapy via spraying condition. (A) The two step modification was performed on chitosan backbone in Milli-Q water. In situ green aqueous crosslinking was initiated using glutaraldehyde to form nanogels that encapsulate p-CA. The nanogels were then purified via dialysis and tested for their multiple effectiveness. (B) The schematic illustration show how the nanogels are effective towards the wound area. (C) The multiple effectiveness of nanogels were further illustrated such as: 1) reduction of cellular ROS level, 2) antimicrobial efficacy, 3) *in vitro* wound healing, 4) protein antifouling effect, 5) reduction of anti-inflammatory marker (e.g. NO).

heightened antioxidant and antibacterial capabilities due to the incorporated sulfobetaine and p-coumaric acid, facilitating accelerated wound closure and reduced inflammation. These strategies ensure stability of the nanogels during long-term storage and high biocompatibility under physiological conditions, while their green aqueous synthesis approach minimizes environmental impact. Encouraging results from *in vitro* wound healing models affirm the potential of modified CS-based nanogel therapy for effective wound care management.

2. Materials and methods

2.1. Materials

All materials were used without further purification. Low molecular weight CS (Mw = 50,000–190,000 Da), TNBS, GA, DMAPS (>95 %), p-Coumaric acid (≥98.0 %), EDC (≥98.0 %), NHS (98 %), acetic acid (≥98 %), BSA protein, Total Antioxidant Capacity Assay Kit, ABTS™ (≥98 %), and DPPH were purchased from Sigma-Aldrich. Micro-BCA™ Protein Assay Kit was from Thermo Fisher Scientific. Deuterium oxide solution, Folin & Ciocalteu's phenol reagent, CCK-8 assay, PBS (150 mM), DMEM, FDA (cell culture grade), PI (≥94.0 %), RAW 264.7 cells, and HDF (adult) were used as received.

2.2. Synthesis of zwitterionic sulfobetaine modified chitosan (Z-CS)

Sulfobetaine-functionalized CS was synthesized *via* Michael addition (Figure S1). Under N_2, DMAPS (0.61 g, 2.3 mmol) in 5 mL Milli-Q water was added dropwise to CS (0.5 g, 5.1 mmol glucosamine unit) in 1 mL of 0.1 wt% acetic acid. The reaction was stirred at 0 °C for 30 min, then the pH was adjusted to ~7.4 with 1.0 M NaOH. Stirring continued for 2 h at room temperature and 8–10 h at 80 °C. The mixture was centrifuged (5000 rpm, 10 min) and washed 5–7 times. Excess sulfobetaine was removed by dialysis (MWCO: 3.5–5 kDa) against Milli-Q water for 2 days. The final product was isolated by lyophilization.

2.3. Synthesis of p-CA modified chitosan (ZC-CS)

Z-CS (1.02 mmol glucosamine unit) was dissolved in 4 mL Milli-Q water and stirred at 450 rpm for 2 h at room temperature. A solution of 175 mg p-CA, 1.42 mmol EDC, and 1.42 mmol NHS in 5 mL Milli-Q was added. The reaction proceeded for 24 h at 450 rpm. The material was precipitated, centrifuged (5000 rpm, 5 min), washed with Milli-Q water, and dialyzed (MWCO: 3.5–5 kDa) against Milli-Q water for 1 day. The product was isolated by lyophilization.

2.4. Amino density test

TNBS assay

CS, Z-CS, and ZC-CS samples were dissolved in 1 mL of 0.01 M HCl. 200 µL of each solution was mixed with 300 µL of 8 % $NaHCO_3$ and 500 µL of 0.1 % TNBS (diluted 100x in Milli-Q). The mixtures were incubated in the dark for 2 h at 37 °C. Absorbance of 200 µL of each sample was measured at 345 nm (Table S1). The standard curve was created using cysteine hydrochloride solutions in 0.5 % sodium chloride, with a cysteine-free solution as a reference. Each sample was measured three times.

2.5. Solubility test of modified CS in aqueous media

The solubility of CS, Z-CS, and ZC-CS in Milli-Q and PBS was measured at 25 °C. Samples of different concentrations were dissolved in equal volumes of Milli-Q water, shaken at 350 rpm for 24 h, then sonicated and centrifuged at 3000 rpm for 15 min. The precipitate was analyzed in PBS and suitable dilutions with Milli-Q. Solubility results are in Table S2.

2.6. Synthesis of CSNG

Nanogels were prepared as shown in Fig. 1. CS (20 mg) was dissolved in Milli-Q, then GA (200 µmol) was added, and the mixture was stirred at 25 °C for 3 h at 450 rpm. The GA amount varied from 200-400 µmol while CS remained constant (Table 1). After crosslinking, nanogels were purified by dialysis (MWCO: 0.5–1 kDa) against Milli-Q water for 24 h and freeze-dried for further characterization.

2.7. Synthesis of zwitterion p-CA CSNG (ZC-CSNG)

ZC-CSNG were prepared similarly. An aqueous solution of ZC-CS (~35 mg) was mixed with various GA concentrations and stirred at 25 °C for 3 h at 450 rpm. The GA molar ratio varied from 200-400 µmol while ZC-CS concentration remained constant (Table 1). After crosslinking, the nanogels were purified by dialysis (MWCO: 0.5–1 kDa) against Milli-Q water for 24 h and freeze-dried for further characterization.

2.8. Instruments and characterization

NMR (Bruker Ascend™ 400 MHz) analyzed CS, Z-CS, and ZC-CS in D2O. *FTIR (Thermo Fisher Nicolet)* recorded spectra of freeze-dried samples. *UV–vis (Tecan Spark®)* measured absorbance and fluorescence. *XRD (Huber G670)* collected patterns (2θ range 3-100°, CuKα1 radiation) from a rotating sample.

Degree of crystallinity (%) = The crystalline index (CI; %) was obtained from the intensity ratio of the crystal phase to the total phase of crystal and amorphous phase in XRD patterns using Equation (1):

$$CI_{110} = \frac{I_{110} - I_{am}}{I_{110}} \times 100 \quad (1)$$

where I_{110} is the maximum intensity at the angle of the lattice diffraction at 20°; i.e., the sum of amorphous and crystalline diffraction, and I_{am}, the intensity of amorphous diffraction at 16°.

X-ray Photoelectron Spectroscopy (XPS): Thermo Scientific's XPS K-Alpha analyzed freeze-dried CS, Z-CS, and ZC-CS with a monochromated Al Kα X-ray source (1486.6 eV) under ultrahigh vacuum (~8×10^{-6} mbar). *Differential Scanning Calorimetry (DSC):* TA-DSC Q-200 (USA) assessed thermal properties, heating samples (3–5 mg) from 0 °C to 400 °C at 10 °C/min in nitrogen (50 mL/min), plotting heat flow versus temperature. *Thermogravimetric Analysis (TGA):* TA Instruments TGA Q500 monitored mass loss of dried samples (CS, Z-CS, ZC-CS) from 30 to 900 °C at 10 °C/min under constant nitrogen flow (60 mL/min).

Size and ζ potential. Particle size, PDI, and Zeta potential of CSNG and ZC-CSNG were measured by DLS Zetasizer ZS (Malvern Instruments, UK) at a scattering angle of 173°. Prior to measurement, nanogel concentration was adjusted to 2.0 mg/mL using Milli-Q water and PBS. Particle diameter was calculated using the Stokes–Einstein equation (2).

$$D = \frac{kT}{6\pi\eta D_t} \quad (2)$$

Table 1
Nanogel synthesis condition optimization using GA cross-linker at room temperature. The concentration of chitosan (CS) and modified chitosan (ZC-CS) fixed and cross-linker were varied and the remaining constituents were kept constant.

S. No	CS/ZC-CS (µmol)	GA (µmol)	Yield%
CSNG-1	200	200	56
CSNG-2	200	300	69
CSNG-3	200	400	73
ZC-CSNG-1	42	200	64
ZC-CSNG-2	42	300	77
ZC-CSNG-3	42	400	81

where, k is Boltzmann's constant, T is temperature in K, and η is solvent viscosity. All measurements were repeated thrice with 16 scans. Mean and SD of triplicate measurements were reported. Gelation in CSNG-1 and ZC-CSNG-1 samples was characterized by recording total scattering intensity of 100 μL samples at different time points.

Transmission electron microscope (TEM). Nanogel morphology was observed *via* transmission electron microscope (TEM). 5 μL of aqueous solution (~1-1.5 mg/mL) was placed on a freshly glow-discharged lacey carbon on 300 mesh copper TEM grid (TedPella, Redding California), blotted, and plunge-frozen in liquid ethane using a Leica EM GP2 plunge freezer (Leica, Germany). Samples were imaged using a FEI Tecnai G2 20 TEM (ThermoFischerScientific) operated at 200 keV in low dose mode with a TVIPS XF416 CCD camera at DTU Nanolab. TEM micrographs were processed using Image J software.

2.9. Stability study

Stability of CSNG and ZC-CSNG was assessed by DLS for hydrodynamic size and PDI. Nanogels were stored at both 25 °C and 4 °C for 28 days. Samples were examined on the 7th, 14th, 21st, and 28th day to monitor changes in particle size, appearance, sedimentation rate, and redispersibility.

2.10. Determination of active phenol (–OH)

Folin-Ciocalteu (F-C) Assay

Total phenolic content in ZC-CSNG was determined using FC reagent, expressed as tyramine equivalents. A 100 μL solution of ZC-CSNG (0.02–0.10 wt/v%) was mixed with 2.5 mL 10 % (*v/v*) FC reagent and 2.5 mL 7.5 % (w/v) Na_2CO_3 in Milli-Q. A blank solution contained 100 μL Milli-Q, 2.5 mL 10 % (*v/v*) FC reagent, and 2.5 mL 7.5 % (*w/v*) Na_2CO_3 in Milli-Q. Samples were incubated at 37 °C for 60 min, then absorbance at 765 nm of phosphomolybdic acid complexes was measured. Active phenol (–OH) of p-CA conjugated CS (ZC-CSNG) was expressed as p-CA equivalent using a standard curve.

2.11. Antioxidant/Anti-ROS activity assay

(A) Total antioxidant capacity assay (TAC):

The total antioxidant capacity assay kit (Sigma-Aldrich, MAK187) analyzed TAC of synthesized CSNG and ZC-CSNG, with CSNG as control. Cu^{2+} reagent was diluted with 49 parts assay diluent. Trolox standard (1 mM) was prepared by mixing 20 μL DMSO solution with 980 μL MQ water. A standard curve was generated using diluted Trolox samples with Cu^{2+} solution. UV-absorbance at 570 nm ($A_{570\ nm}$) of various concentrated nanogels dissolved in Milli-Q water was measured. Measurements were triplicated and repeated thrice. Antioxidant amount was calculated using the Trolox standard curve, and Total antioxidant concentration was determined using an equation (3):

$$Sa/_{Sv} = \text{Concentration of antioxidant in each sample} \quad (3)$$

Sa = Trolox equivalent of unknown sample well (nmol) from standard curve

Sv = Sample volume (μL) added into each well.

(B) Antioxidant activity assay by ABTS$^{\bullet+}$

The $ABTS^{\bullet+}$ assay relies on the ability of antioxidants to neutralize the ABTS radical cation, with a characteristic absorption peak at 745 nm. CSNG and ZC-CSNG (0.05–0.25 *w/v*%) were introduced into 10 mL pH 7.4 PBS, with CSNG as control. $ABTS^{\bullet+}$ was generated by mixing 2 mM ABTS with 2.45 mM potassium persulfate in PBS and incubating in darkness at room temperature for 5 h. The resulting solution was diluted in pH 7.4 PBS for absorbance at 745 nm. Then, 1 mL of the diluted $ABTS^{\bullet+}$ solution was combined with 3 mL of nanogel solution. After 30 min, percentage inhibition of $ABTS^{\bullet+}$ at 745 nm was calculated relative to control using the equation (4):

$$ABTS^{\bullet+}\text{scavenging effect}(\%) = \left(1 - As/_{Ac}\right) \times 100 \quad (4)$$

where As is the absorbance of the remaining $ABTS^{\bullet+}$ in the presence of p-CA conjugated nanogels, Ac is the absorbance of the initial $ABTS^{\bullet+}$ concentration. The standard curve was created using various p-CA concentrations.

(C) DPPH free radical scavenging activity.

To assess scavenging activity, we monitored DPPH reduction in the presence of ZC-CSNG. Swollen ZC-CSNG was introduced into 10 mL pH 7.4 PBS. At intervals (30, 60, 90, 120, and 240 min), 200 μL of PBS medium was extracted and dried overnight at 37 °C. Then, 1.5 mL ethanol was added to dried nanogels, vortexed for 2 min, and incubated for 20 min. Next, 0.5 mL 0.1 mM DPPH solution in ethanol was added, vortexed vigorously, and left in the dark for 30 min before measuring absorbance at 517 nm relative to PBS control. Ethanol served as baseline correction. Radical scavenging effect was calculated by the equation (5):

$$DPPH^{\cdot}\text{ scavenging effect}(\%) = \left(1 - A0/_{A1}\right) \times 100 \quad (5)$$

where, $A0$ is the absorbance in the presence of p-CA in the nanogels and $A1$ is the absorbance of the control which contains DPPH solution.

(D) Reducing power assay.

ZC-CSNG or CSNG were added to 10 mL PBS (pH 7.4). Samples ranging from 0.1 % to 0.5 % (*w/v*%) were prepared, with 200 μL withdrawn and mixed with 800 μL PBS in a falcon tube. Then, 5 mL 0.2 M PBS (pH 7.4) and 5 mL 1 % potassium ferricyanide were added, and the mixture was incubated at 50 °C for 25–30 min. Next, 5 mL 10 % trichloroacetic acid was added, followed by centrifugation at 1000 rpm for 10 min. The upper supernatant (5 mL) was combined with 5 mL distilled water and 1 mL $FeCl_3$ (0.1 %) using vortex mixing. Absorbance was measured against a water blank at 700 nm using a spectrophotometer, with increased absorbance indicating improved reduction capability. Experiments were conducted in triplicate.

(E) Hydroxyl radical-scavenging ability assay.

We followed Liu's protocol [44] with slight modifications to evaluate the capacity to scavenge hydroxyl (˙OH) radicals. To quantify ˙OH radical generation *via* Fenton reagents, we used H_2O_2 oxidation. PBS (pH 7.2) and sample solutions ranging from 0.05 % to 0.4 % (*w/v*%) were prepared. A solution containing H_2O_2 (3 %) and safranine O (360 μg/mL) in PBS (pH 7.4) and Fe^{2+} (2 mM) in Milli-Q water was also prepared. The reaction mixture (4.5 mL) included sample solution (0.022 to 0.18 mL), water (0.978 to 0.82 mL), Fe^{2+} solution (0.5 mL), safranine O (360 μg/mL), and H_2O_2 (1 mL) in PBS, incubated at 37 °C for 30 min. ˙OH concentration was set at 120 μM, and absorbance was measured at 520 nm. Blank samples used Milli-Q water instead of samples, while PBS replaced H_2O_2 in negative controls. Three replicates were conducted for each sample, and the ability of the products to neutralize ˙OH radicals was calculated using a specific equation (6):

$$\text{Scavenging}(\%) = \frac{A_{s,520nm} - A_{b,520nm}}{A_{c,520nm} - A_{b,520nm}} \quad (6)$$

where, $A_{b,520nm}$ is the absorbance of the blank at 520 nm; $A_{s,520nm}$ is the absorbance of the sample at 520 nm; and $A_{c,520nm}$ is the absorbance of the control at 520 nm.

2.12. Protein antifouling test

Test ran at 37 °C. 2.5 mg CSNG and ZC-CSNG, 500 μg BSA dispersed in 1 mL Milli-Q water, vibrated gently for 120 min. ZC-CSNG also tested with 1 mL 150 mM NaCl. Nanogels washed with Milli-Q water, filtrate collected for protein quantification using micro-BCA assay kit. After protein incubation, samples filtered and washed 3 times with original solutions using Amicon® Ultra-centrifugal filters (100 kDa MWCO) to

remove unabsorbed proteins. Absorbance of samples measured at 562 nm. Non-recovered protein considered adsorbed to nanogels. Nanogel hydrodynamic size determined at different time points (0 min, 1 h, 2 h) with DLS.

2.13. In vitro cell culture

Cell growth conducted in humidified 5 % CO_2, 37 °C incubator. RAW 264.7 cells cultured in PS cell culture flask (5×10^5 cells per well) in Dulbecco′s Modified Eagle′s Medium – high glucose, supplemented with 10 % FBS and 1 % penicillin. Cells sub-cultured every 2–3 days with fresh media. For Human dermal fibroblast (HDF) cell growth, DMEM-high glucose used (supplemented with 10 % FBS, 1 % penicillin/streptomycin). Cells sub-cultured every 3–4 days, fresh media replenished every 48 h.

2.14. Cytotoxicity study and Live/Dead HDF cell staining

The cytotoxicity of the nanogels were assessed *via* CCK-8 assay with HDF cells. CSNG and ZC-CSNG applied to well plate, incubated with DMEM (10 % FBS, 1 % penicillin/streptomycin) for 24 h. Conditioned medium tested on HDF cells (passage 3–4). For the assay, 3.5×10^4 cells seeded in 96-well plates, incubated for 24 h. Medium replaced with nanogel conditioned medium, incubated for another 24 h. CCK-8 solution added, absorbance measured at 450 nm using Tecan microplate reader, with Triton X-treated cells as positive control. Differentiation of viable HDF cells post-treatment with nanogel conditioned medium (CSNG and ZC-CSNG) achieved through FDA and PI staining. HDF cells seeded on treated slides, exposed to nanogels for 24 h, then stained with FDA and PI. Imaging conducted using Nikon Ti_2 inverted spinning disc confocal microscope. Triton X-100 used as positive control, incubated with HDF cells for 10 min.

2.15. In vitro antibacterial assays

Microorganisms and culture media

Staphylococcus aureus CCUG10778 and *Staphylococcus epidermidis* ATCC 35984 were used to determine the antimicrobial activity. Both the strains were grown in LB (Luria-Bertani) liquid medium.

2.16. Minimum inhibitory concentration (MIC) and minimal Bactericidal concentration (MBC) determination

MIC of ZC-CSNG was determined by using an overnight incubated culture of *S. aureus* and *S. epidermidis*. The bacterial cultures were diluted to reach $1–2 \times 10^5$ (CFU)/mL, 100 μL of it were mixed with a serial dilution of ZC-CSNG in the concentration range 0.2 to 2 mg/mL. The samples were incubated at 37 °C for 24 h, and then OD_{550} was measured. The MIC was defined as the lowest concentration of ZC-CSNG, which inhibited bacterial growth. For determining the MBC, 100 μL of mixtures described above were spread on agar plates and incubated at 37 °C overnight. MBC value was defined as the lowest concentration of ZC-CSNG, which prevented the visible growth of bacteria on agar plates.

2.17. Live and dead bacterial cell staining

To visualize the viable and dead cells, control cells and cells treated with ZC-CSNG were stained for 20 min with a mixture of 6.0 μM SYTO 9 and 30 μM KI from Live/Dead BacLight Viability kit L13152, (Invitrogen, Molecular Probes, Inc. Eugene, OR, USA). Fluorescence microscopic imaging of the cells was performed using a LEICA DM 4000B (Leica Microsystems, Denmark).

2.18. Scanning electron microscopy (SEM) bacterial cell analysis

SEM was performed by fixing the control and treated cells with 3 % of GA overnight at 4℃ and dehydrated with graded series of ethanol concentrations (40, 50, 60, 70, 80, and 90 % for 15 min each and with absolute ethanol for 20 min. The dehydrated samples were dried at room temperature overnight and coated with gold before SEM imaging, performed with a Quanta FEG 200 ESEM microscope (ThermoFisher Scientific).

2.19. In vitro HDF cell migration assay

Adult HDF cells were grown to approximately 90 % confluence in 12-well plates, rinsed with PBS, and starved for 24 h using DMEM containing 10 % FBS. Subsequently, a simulated wound (scratch) was created across the cell layer using a 200 μL pipet tip at the well's base and cleaned with medium to remove cell debris. In a separate step, ZC-CSNG mixture (200 μL) was placed in a well plate, solidified, washed with 1X PBS, and incubated in DMEM with 10 % FBS (800 μL) for 24 h. The nanogel conditioned medium (1.2 mL) was then introduced into the wells containing the scratched cell layers. As a control, scratched cell sheets were treated with DMEM with 10 % FBS (1.2 mL). Phase-contrast microscopy images of both treated and untreated cells were captured at 0, 24, and 48 h, allowing for visual comparison to monitor differences in cell migration behavior.

2.20. Sprayable nanogels formulation

ZC-CSNG nanogel was dissolved to ~60 mg/mL in Milli-Q. A similar concentration of native CS was used as control. The sample solution in the shaker was sonicated before spraying. Each round of sprayed nanogels were collected in a cuvette, dissolved in 1 mL Milli-Q and analyzed by DLS & TEM. The released mass fraction (wt/v%) in each cycle after freeze drying is reported.

2.21. Anti-inflammatory marker assay

To evaluate the anti-inflammatory properties of the nano-hydrogel, we employed a "Griess assay" to measure the release of nitric oxide (NO) as nitrite. A mixture of nanogel precursors (100 μL) was applied to a well plate, allowed to solidify, rinsed with 1X PBS, and incubated with DMEM containing 10 % FBS (1 mL) for 24 h. Meanwhile, RAW 264.7 macrophages were seeded at a density of 2.3×10^4 cells/well and allowed to reach confluence within 24 h. To stimulate NO production, 100 ng/mL of lipopolysaccharide (LPS) was added to each well. After 6 h, nanogel-conditioned medium (100 μL) was introduced into each well and incubated for another 24 h. Positive controls consisted of cells treated with LPS alone, while negative controls consisted of untreated cells (no LPS or conditioned medium). Following the 24-hour incubation, RAW 264.7 cells were centrifuged, and the supernatants (100 μL) were transferred to a 96-well plate, along with 100 μL of Griess reagent prepared as per the manufacturer's protocol. After a 15-minute incubation, the quantity of NO was determined using a microplate reader by measuring UV absorbance at 540 nm. All experiments were performed in triplicate.

2.22. Hemolysis test

Hemolysis test evaluates acute hemolysis *in vitro*. Whole blood mixed with buffer media, centrifuged, and washed. Pellet resuspended in PBS, then mixed with CS/ZC-CSNG solution. Incubated at 37 °C for 1–2 h, followed by centrifugation. Absorbance of supernatant at 540 nm measured to calculate hemolysis rate. Positive and negative controls used blood cells in MQ water or buffer, respectively. Hemolysis rate calculated using equation. (7)

$$\text{hemolysis rate}(\%) = \frac{A_{s,540nm} - A_{b,540nm}}{A_{c,540nm} - A_{b,540nm}} \quad (7)$$

2.23. Statistical analysis

Data are presented as mean ± standard deviation (SD) and each sample was analyzed 3 times.

3. Results and discussion

In order for ZC-CSNG to demonstrate potential to serve as an agent promoting wound healing, they must fulfill a range of characteristics, such as anti-inflammatory properties, dermal cell compatibility or ideally, promotion of dermal cell proliferation, and anti-bacterial efficacy. The nanogel particles (NGs) as well as the polymers from which they are synthesized, must be well characterized and stable. Here, we describe the synthesis and characterization of NGs, focusing on antioxidant properties, free radical scavenging, reducing capacity, as well as NO-suppression and anti-bacterial response. The NGs must not be toxic towards the cells and they must remain unaltered in the wound. Thus, the investigation includes cytotoxicity and protein fouling assessments. Finally, the investigation explores the sprayability of the NGs.

Table 2, above highlights how our study on ZC-CSNG advances the field compared to previous research [45–49]. Unlike prior studies, our work integrates zwitterionic modification and Schiff base crosslinking with antioxidant functionality into a sprayable nanogel system. This approach significantly enhances solubility, protein antifouling, antibacterial activity, and ROS scavenging, making our nanogels uniquely suited for wound dressing applications. Additionally, our green synthesis method ensures biocompatibility and environmental sustainability.

3.1. Synthesis and characterization of zwitterion p-CA modified ZC-CS

An organic solvent free, step by step "green synthesis" approach was employed for amine modification of CS, as illustrated in Figure S1. A two-step modification was carried out in aqueous media and purified using dialysis techniques. CS was modified with a sulfobetaine methacrylate moiety *via Michael addition* and with p-CA *via* EDC/NHS amide coupling at room temperature to obtain Z-CS and ZC-CS, respectively. Z is Zwitterion and C is p-coumaric acid. ^{1}H NMR are in accordance with the structure given in Fig. 1 (see supplementary information Figures S2, S3, and S4). As expected, the free amine content was reduced following successful modification at each step (see Table S1).

ATR FTIR-spectra of CS, Z-CS, and ZC-CS (Fig. 2A,B) exhibit two bands associated with the sulfobetaine functional group: a band at 1468 cm^{-1}, corresponding to $–N^+(CH_3)_2–$ bending and a band at 728 cm^{-1} due to S–C stretching. Typical characteristic peaks of the sulfonate group $–SO_3^-$ at 1156 cm^{-1} (asymmetric st.) and 1033 cm^{-1} (symmetric st.) is seen in Z-CS and ZC-CS. ZC-CS also showed a peak at 1513 cm^{-1} due to C═C stretching in the aromatic ring of p-CA [50]. An ester peak at 1724 cm^{-1} due to the bonding of the sulfobetaine is present in both Z-CS and ZC-CS. The amide bond is associated with the p-CA bonding bands in both the amide-II region (1561 cm^{-1}) and the amide-I region (1667 cm^{-1} to 1638 cm^{-1}) is in accordance with amide bond attachment of p-CA using EDC/NHS coupling. Finally, the FTIR spectra show the expected bands associated with the CS polymer backbone: 3367 cm^{-1} –OH and $–NH_2$, 2869 cm^{-1}C-H stretching, 1081 cm^{-1} deformation of the –C–O–C– link of the glycosidic bonds and 894 cm^{-1} pyranose ring [51]. Furthermore, the band shift at 3367 cm^{-1} to 3270 cm^{-1} is in accordance with the expectation for$–NH_2$ modification. Thus, the FTIR data is in accordance with the successfully modification of CS to Z-CS and ZC-CS.

Modification have been reported to have a great influence on the thermal properties of CS. DSC thermograms of CS, Z-CS and ZC-CS are shown in Fig. 2C, followed by TGA (Fig. 2D). The initial weight loss at ~50°C and the initial endothermic DSC peaks represent loss of water. This is followed by the glass transition at ~130 °C visible in the DSC traces for CS and Z-CS (no TA signal). Finally thermal decomposition gives a substantial weight loss in TGA and endothermal peak in the DSC. The thermal stability decreases through the order CS, Z-CS, to ZC-CS. The TGA traces can be interpreted as distinct degradation mechanism associated with the p-CA functionality (at ~ 150 °C) and the sulfobetaine functionality (at ~ 220 °C) and finally CS main chain degradation at ~280 °C.

In the solid phase, CS is a semi-crystalline polymer, as evidence by the peaks in the XRD pattern (Fig. 2E) at 2θ values of 10.12° and 19.95°, which corresponds to the lattice planes [52] and [1 1 0], respectively, in the orthorhombic crystal [53]. The degree of crystallinity in CS is ~62 %. The introduction of side-chain functionalizations completely suppresses crystallinity in Z-CS and ZC-CS, as evidenced by the absence of crystalline peaks and the presence of a broad amorphous signal. The survey XPS spectra in Fig. 2F of the CS, Z-CS, and ZC-CS show the presence of the expected elements (C, N, and O) in CS samples, with S being present only in Z-CS and ZC-CS. High resolution spectra are given in Figure S6. CS is considered as a difficult to dissolve in aqueous media biocompatible material. Solubility test at various pH was tested (see Table S2). Native CS was insoluble in Milli-Q and buffered and dissolves only at low concentration in acidic solution (Figure S7) probably due to amino group protonation. As expected, zwitterion modification promotes solubility at all pH-values, thereby improving processability.

3.2. Nanogel synthesis and characterization

Crosslinking with GA is employed to safeguard the activity of p-CA

Table 2
Comparative analysis of chitosan-based materials for biomedical applications.

S. No	Study Focus	Key Innovations	Comparative Features	Highlights in this work	Reference
1	Modified chitosan for wound healing	Improved mechanical properties and enhanced drug release	Similar focus on wound healing; different methods and materials	Zwitterion-modified chitosan-based nanogels with multifunctional properties and enhanced solubility	[48]
2	Biodegradable chitosan composites for biomedical use	Development of biodegradable composites	Comparable material, different application focus	Sprayable nanogels with enhanced solubility and antioxidant functionality	[45–46]
3	Nanoparticle-loaded chitosan for drug delivery	Incorporation of nanoparticles for targeted delivery	Similar material base; different delivery mechanism	Nanogels with integrated zwitterionic and antioxidant functionalities for wound care	[49]
4	Functionalized chitosan for tissue engineering	Advanced functionalization techniques for improved cellular interactions	Similar functionalization, different applications	Green synthesis of multifunctional nanogels with enhanced ROS scavenging and antibacterial properties	[47]
5	Sprayable zwitterion-modified chitosan nanogels for wound dressing	Zwitterion modification, Schiff base crosslinking, antioxidant incorporation, green synthesis	New formulation with enhanced solubility, protein antifouling, antibacterial activity, and ROS scavenging	Multifunctional sprayable nanogels with superior solubility, prolonged stability, and comprehensive wound care properties	This Work (ZC-CSNG)

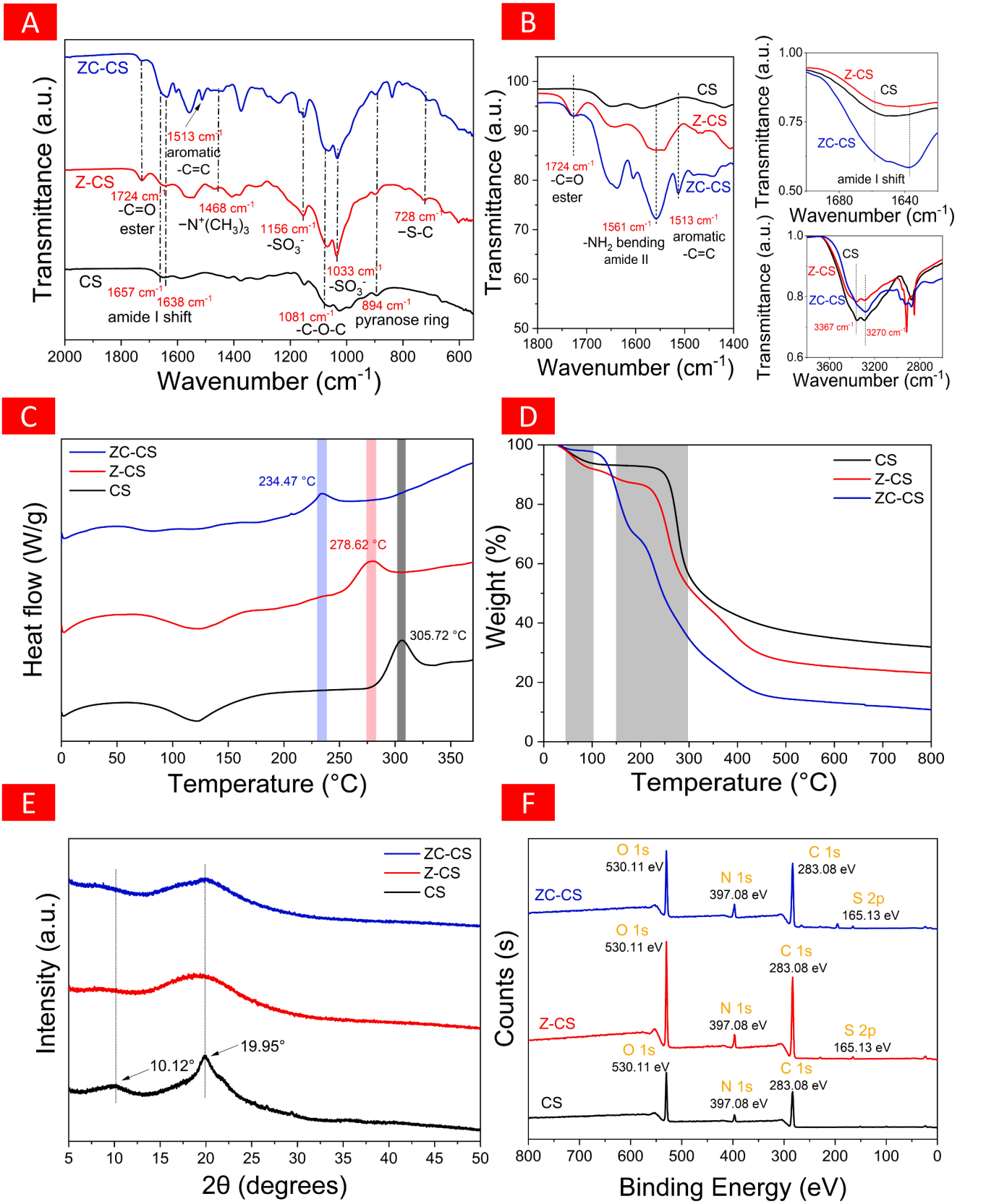

Fig. 2. Structural characterization of native CS and modified CS. (A) ATR-FTIR spectra of CS, Z-CS and ZC-CS. (B) Zoom of FTIR spectra: main peaks evaluated for the CS, Z-CS and ZC-CS. (C) DSC diagram analysis of CS, Z-CS and ZC-CS. (D) TGA analysis of CS, Z-CS and ZC-CS. (E) XRD diffraction analysis of CS, Z-CS and ZC-CS. (F) XPS analysis of CS, Z-CS and ZC-CS.

within the hydrogel matrix. The GA reacted with free amine groups on chains of CS, Z-CS, and ZC-CS to form Schiff base linkages. Crosslinked nanogels are often synthesized using heterogeneous polymerization employing organic solvents and emulsifiers; however, we have developed a "green aqueous synthesis approach." A series of nanogels have been synthesized by imine formation at room temperature. The nanogels were synthesized by one-pot mixing all the required constituent such as CS, Z-CS, or ZC-CS and *in situ* gelling was initiated using GA at 25 °C under magnetic stirring to obtain CS-NG and ZC-CSNG as shown in Table 1 followed by dialysis purification. The crosslinking reaction was followed with FTIR, (Fig. 3A). A Schiff base line appears at 1652 cm^{-1}. The lines associated with the zwitterionic and p-CA functionality is at 1468 cm^{-1}, 1156 cm^{-1}, and 1513 cm^{-1} are intact. Due to the water solubility of GA purification by dialysis is easy.

Following gelation, the total light scattering is recorded, I_{173° (Fig. 3B) in preparation of CSNG-1 and ZC-CSNG-1. Since $I_{173^\circ} \sim cM_w$ and as the polymer concentration is constant I_{173° is a proxy for the molecular weight of the particles, we conclude that the reaction has reach conclusion after 3 h. Similarly, an increase in particle size was also observed when the free amine/GA ratio was decreased from 1 to 0.5 (Fig. 3C), which provided a way to control the size of nanogels. As expected less residual free amine led to a decrease in the positive ζ-potential. CSNG-1 show a mean hydrodynamic size of ~178 ± 5 nm and ZC-CSNG-1 slightly smaller. Based on these observations all following experiment were conducted using either CSNG-1 or ZC-CSNG-1 particles. The stability of CSNG and ZC-CSNG is evidenced by the absence of precipitation and the maintenance of size over 4 weeks in 2 mg/mL solution (Figure S8). The hydrodynamic size of ZC-CSNG increased (180 nm to 230 nm) in 150 mM NaCl solution (data not shown). The expansion of the nanogel size is mainly due to the "anti-polyelectrolyte" effect of the poly(zwitterion) segment [54]. Fig. 3D shows TEM images of CS-NG and ZC-CSNG, both exhibiting spherical morphology. A nominal size difference was observed between DLS and TEM analysis, likely due to the hydration effect [55]. The sprayability of ZC-CSNG in Milli-Q was tested by spraying and collecting in a small vial, freeze dried and reconstituted with Milli-Q. The cumulative release of NGs on each spraying cycle is shown in Fig. 3E. The integrity of the particle after spraying is analyzed by DLS and TEM and we observed the preservation of the ZC-CSNG characteristics (Fig. 3F, see in video). Native CS precipitates in the sprayer, leading to negligible release. This property point to a novel strategy of flying swelled nanogels which could open up a mode of local skin care management *via* sprayable gel particles.

3.3. Antioxidant and anti-ROS efficacy of nanogels

The effects of p-CA functionality in the ZC-CSNG are characterized by analyzing as anti-ROS agents, antioxidants, reductants, and hydroxyl radical scavengers. ZC-CSNG anti-ROS efficacy was evaluated using various methods: such as a) Total antioxidant present in the system; b) ROS scavenging activity (e.g., $DPPH^{\bullet}$, $ABTS^{\bullet+}$ and $^{\bullet}OH$ radical scavenging); and c) reducing power assay. Anti-oxidant properties of phenolic compounds are well established (Fig. 4A) [43,56–57]. The phenolic activity of the ZC-CSNG was characterized using F-C assay to analyze nanogel (visualized in Figure S9). CSNG has no such effect. Thus, the expected effective anti-oxidant of p-CA activity is preserved in ZC-CSNG. The Trolox antioxidant standard was also employed for characterizing TAC (Fig. 4B) [58]. Different concentrations (0.1–0.2 wt/v%) of nanogels was used. The results clearly indicated that ZC-CSNG exhibited antioxidant properties in a dose-dependent manner. Hydroxycinnamic acids (such as ferulic, caffeic, sinapic acid, and p-coumaric acid) highly abundant in food have recently gained an increasing interest in health care, because they are known to be potent antioxidants and anti-ROS agents [59–61]. The anti-ROS effectiveness of the nanogels is characterized by ABTS assay (Fig. 4C). In free radical scavenging the $ABTS^{\bullet+}$ is a model of a stable free radical used to determine free radical scavenging activity of natural antioxidants with beneficial effects such as protection of membrane lipids, proteins, and DNA [62]. It is noted that CS itself appears to scavenge oxygen free radicals [63]. The time dependence of the free radical scavenging was investigated, demonstrating that ZC-CSNG effectively scavenges $DPPH^{\bullet}$ and $ABTS^{\bullet+}$ within approximately 3–4 h (Figure S10). ZC-CSNG (maximum scavenging effect 95 %) is substantially more effective than CSNG (maximum scavenging effect 22 %) highlighting the importance of the p-CA functionality ZC-CSNG show increasing $ABTS^{\bullet+}$ scavenging ratio with increased concentration as opposed to the CSNG where the effect is substantially smaller and essential concentration independent. Further utilization of $DPPH^{\bullet}$ free radical scavenging for characterization (Figure S10) reveals that ZC-CSNG achieves more than 90 % scavenging in 3–4 h, surpassing CSNG. The $ABTS^{\bullet+}$ scavenging ability of ZC-CSNG is preserved over storage for 3 months (Figure S11). The reducing power of the nanogels against ferricyanide is shown in Fig. 4D with a similar result as the free radical scavenging abilities discussed above. Hydroxyl radicals are one of the most aggressive ROS and we directly tested the ZC-CSNG activity against CSNG (Fig. 4E). In conclusion the introduction of p-CA substantially enhances the antioxidant and anti-ROS efficacy of the nanogels. The effect is apparently not diminished by the nanogel structure.

3.4. Biocompatibility, protein antifouling, in vitro wound healing efficacy

In order to characterize the necessary biocompatibility [64] of the nanogels with tissue we have examined the properties with respect to cytotoxicity, protein fouling, wound healing, hemolysis, and anti-inflammatory responses. Cell viability was visually confirmed through live/dead staining of HDF cells and compared to control cells (Fig. 5A). In the untreated, metabolically active HDF cells (negative control), vibrant green fluorescence was observed, closely resembling the cells exposed to ZC-CSNG or CSNG conditioned medium. Moreover, the cell morphology remained similar, suggesting minimal cell death.

The biocompatibility of CSNG and ZC-CSNG was tested using adult HDF and RAW 264.7 cells to evaluate cell proliferation and metabolic activity (see Fig. 5B, 5C). HDF cells were chosen for their key role in tissue structure and wound healing [65–66]. However, the macrophages are associated with the inflammatory tissue [67]. After incubating the nanogels in cell media, we utilized the conditioned media for viability tests. Negative and positive controls involved cells in DMEM media and Triton-X, respectively. Both nanogels exhibited robust cell viability at approximately 85 %. There was no significant cell death observed with CSNG, possibly due to its cationic charge. Importantly, ZC-CSNG did not significantly reduce cell viability either.

The zwitterion modification is expected to impart importance [68] anti-fouling properties to the nanogels. Protein fouling of ZC-CSNG was evaluated by exposure to BS A (model protein). The amount of adsorbed protein to the nanogels is quantified by micro-BCA assay, and the nanogel-attached protein is visualized by particle size measurement using DLS. CSNG was used as a control (without zwitterion) for our study. Fig. 5D, shows substantial protein absorption to CSNG, much less absorption to ZC-CSNG and even less absorption in salt solution demonstrating the superior bio-antifouling ability of the nanogels in physiological saline solution as expected tor a zwitterionic polymer [69]. In Fig. 5E, F, it is observed that the size distribution of ZC-CSNG is essentially time-independent during exposure to the protein solution, whereas CSNG changes with time, increasing the apparent size and forming a multimodal distribution indicating aggregation. Cell migration is an intricate biochemical phenomenon where cells shift from one location to another, playing a crucial role in the process of wound healing [70]. The 2D wound scratch model is employed to assess *in vitro* wound healing (see Fig. 6A). Studies have demonstrated that wound healing hydrogels exhibiting enhanced outcomes in the wound scratch assay also exhibit remarkable wound healing effects in living organisms [71]. To assess the ability of ZC-CSNG to stimulate cell migration and proliferation, we employed a conditioned media approach on HDF cells.

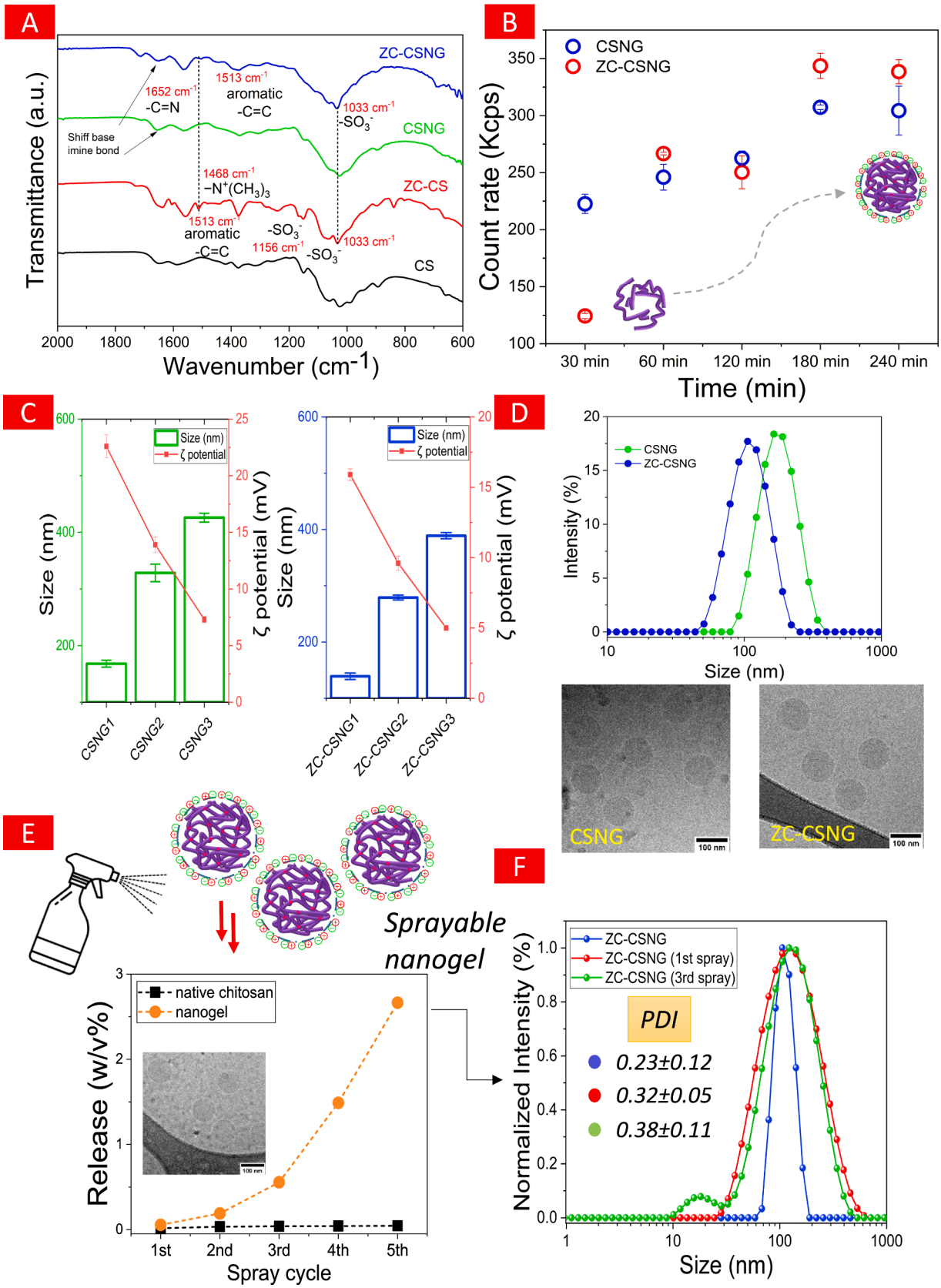

Fig. 3. Characterization and analysis of native CSNG and modified ZC-CSNG. (A) ATR-FTIR analysis of "Schiff base" cross-linked nanogel. (B) Nanogel formation was evaluated by DLS KCPS analysis. (C) Nanogel size (nm) and zeta potential (mV) were evaluated. (D) Nanogels morphology was analysed by TEM. (E) Nanogel release was depicted by spray cycles. (F) Released nanogels stability was analysed by DLS light scattering.

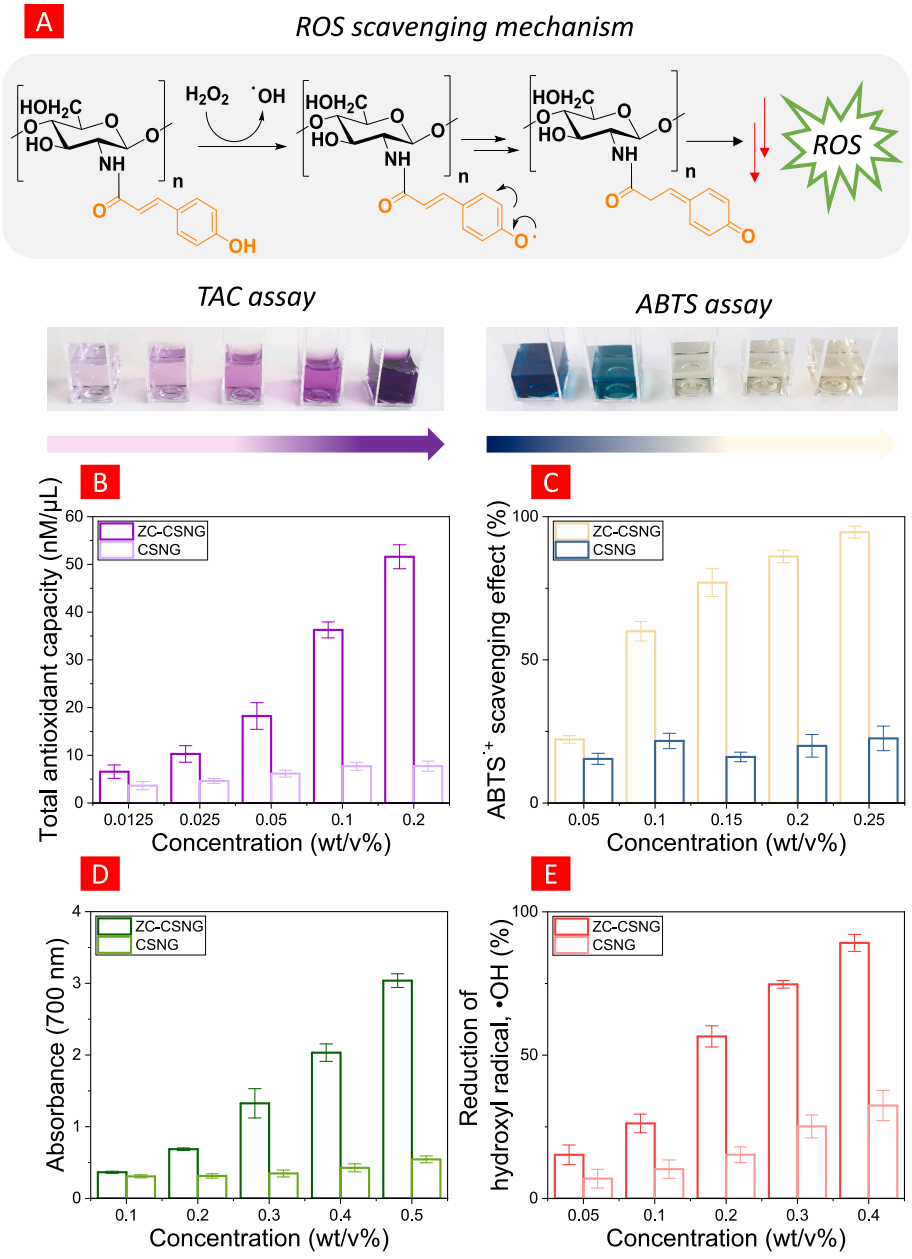

Fig. 4. Antioxidizing effects of ZC-CSNG. (A) Schematic illustration of ROS scavenging mechanism. (B) Total antioxidant capacity (TAC) assay of ZC-CSNG and CSNG (control). (C) $ABTS^{\cdot+}$ ROS scavenging assay of ZC-CSNG and CSNG (control). (D) Reducing power assay of ZC-CSNG and CSNG (control) at 700 nm. (E) Hydroxyl radical ($^{\cdot}OH$) scavenging assay of ZC-CSNG and CSNG (control).

These cells were initially deprived of nutrients for 24 h and then subjected to a simulated wound by manually scratching the cell sheet (as shown in Fig. 6B). Cells require growth factors to encourage replication and prevent apoptosis, typically provided by FBS in DMEM media. After 24 h of incubation without disruption, the HDF cells, now at about 90 % confluence, were scratched to mimic a wound (marked by yellow dotted lines), and the debris was washed away with PBS (Fig. 6B). As shown in Table S3, the effectiveness of ZC-CSNG in promoting wound healing was evaluated using a scratch assay with Human Dermal Fibroblasts (HDF) cells. At 24 h, ZC-CSNG treatment resulted in a 50 % reduction in the scratch area, corresponding to a wound healing rate of 50 %. This is in contrast to the 55 % scratch area and 45 % healing rate observed with CSNG. By 48 h, the scratch area in ZC-CSNG-treated cells was further reduced to 20 %, indicating an 80 % healing rate, which significantly outperformed CSNG, which had a 30 % scratch area and a 70 % healing rate at the same time point. These results clearly demonstrate the superior efficacy of ZC-CSNG in accelerating wound healing, reinforcing its potential as an advanced wound dressing material.

Following this, the remaining cell population was exposed to ZC-CSNG conditioned medium (DMEM with 10 % FBS). Microscopic observations after 24 h revealed substantial cell proliferation and migration, with the scratched area almost entirely covered by a confluent cell layer within 48 h. In contrast, control cells treated with DMEM and 10 % FBS exhibited considerably lower levels of cell proliferation and migration. This experiment provides compelling evidence that ZC-CSNG promotes cell proliferation and migration, suggesting potential benefits for enhanced wound healing. In the process of skin wound healing, inflammatory cells such as neutrophils and monocytes are attracted to the wounded site. They play a crucial role in eliminating bacteria and debris while also promoting the development of granulation tissue and the formation of new blood vessels [72–74]. Nevertheless, the prolonged presence of inflammatory cells results in increased levels of cytokines

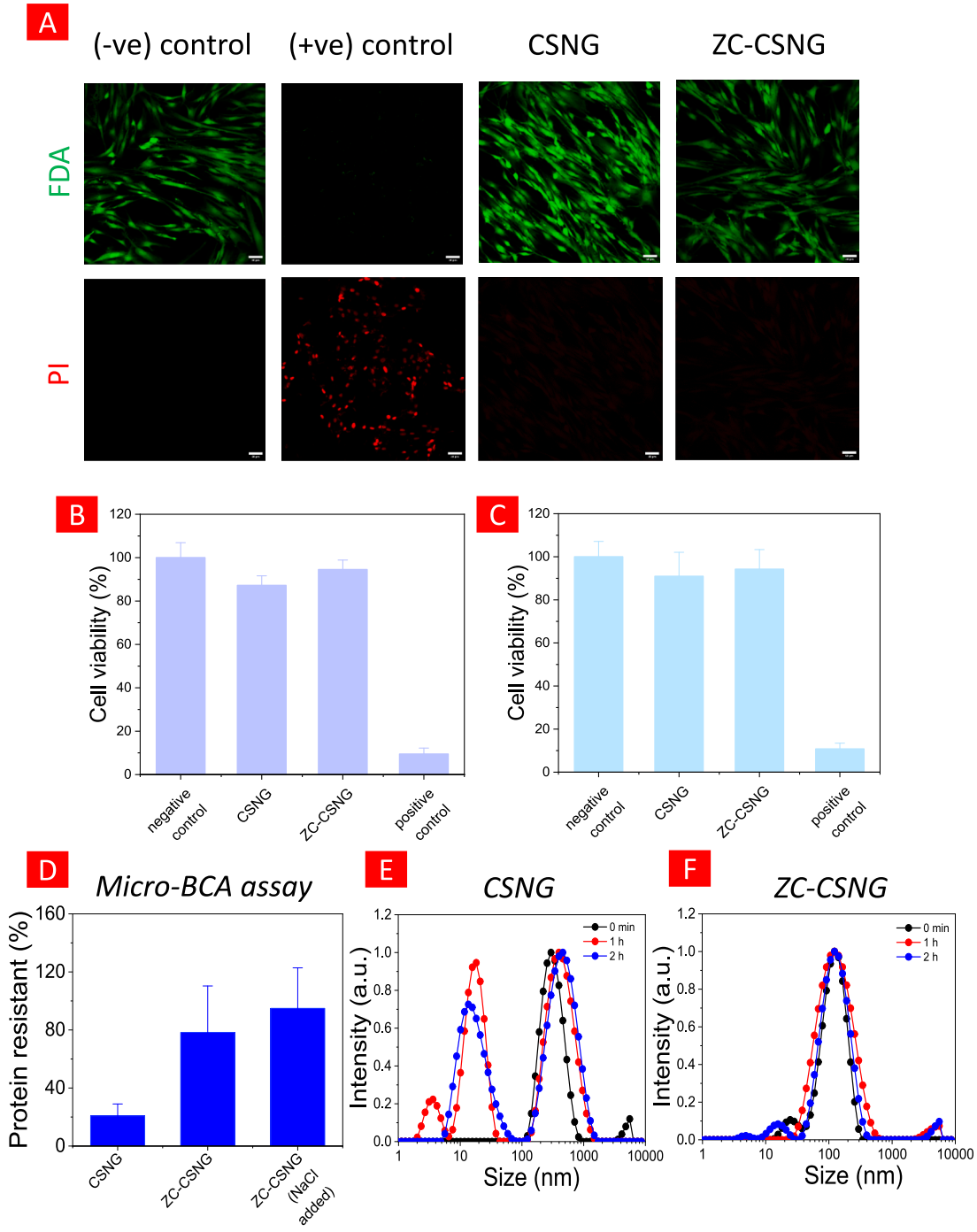

Fig. 5. Cell viability and protein antifouling efficacy of nanogels. (A) Confocal microscopy image of HDF cells incubated with nanogels, where Triton-X is positive control and DMEM buffer in negative control. (−ve): negative; (+ve): positive. (B) HDF cells cytotoxicity assay of ZC-CSNG and CSNG nanogels using WST-8 assay. (C) Macrophage cells cytotoxicity assay of ZC-CSNG and CSNG nanogels using WST-8 assay. (D) Protein anti-fouling activity study of CSNG and ZC-CSNG (using BSA as a model protein) via micro-BCA assay. (E)-(F) Protein anti-fouling activity study of CSNG and ZC-CSNG (using BSA as a model protein) via Dynamic light scattering.

(like IL-6 and TNF-α). These cytokines trigger the production of enzymes that break down tissue, potentially leading to prolonged inflammation that hinders the healing process [75]. Hence, wound dressings containing anti-inflammatory elements hold promise for mitigating this reaction and creating a conducive environment for wound healing. We anticipate that ZC-CSNG, due to its phenolic content, may possess potential anti-inflammatory properties [76].

Mammalian cells produce and release nitric oxide (NO), which plays a vital role in the development of inflammation [77]. Nitric oxide (NO) acts as a pro-inflammatory agent, inciting inflammation in abnormal situations. This characteristic makes it a compelling target for treating inflammatory diseases. Macrophages can be triggered by lipopolysaccharide (LPS), an external stimulus, leading to the excessive production of NO (refer to Fig. 6C) [78–79]. The influence of CSNG and ZC-CSNG on the release of NO was measured (Fig. 6D). ZC-CSNG conditioned medium could suppress NO production suggesting a potential therapeutic effect (Fig. 6D) [80]. Hemolysis assay was performed as an easy and trustworthy approach to evaluate blood cyto-compatibility of nanogels.

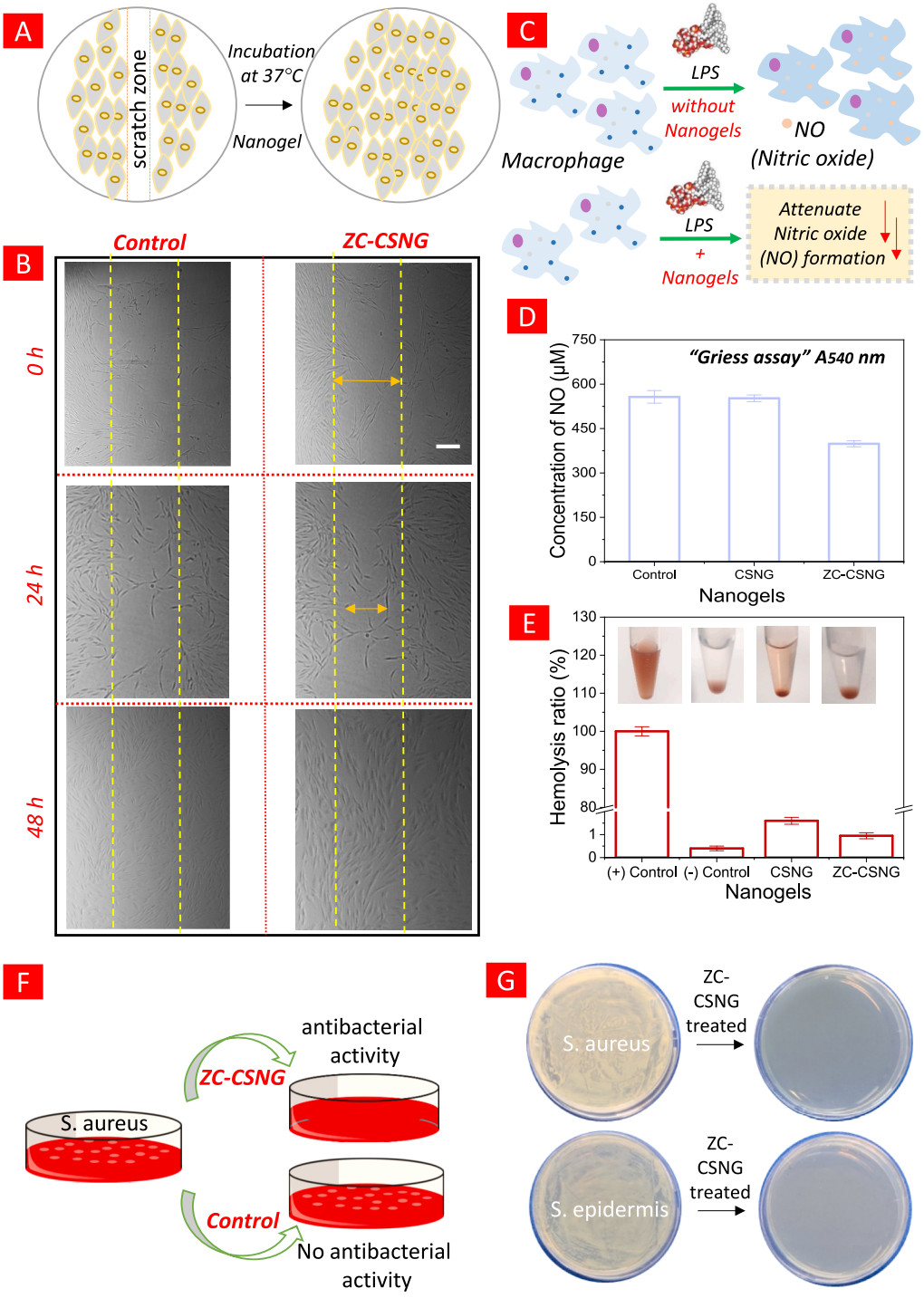

Fig. 6. *In vitro* wound healing, anti-inflammatory and antimicrobial efficacy of nanogels. (A) Schematic illustration of *in vitro* wound healing of HDF cells using nanogel therapy. (B) HDF cells *in vitro* wound healing assay (scratch assay) was performed using nanogels. (C) Schematic illustration of *in vitro* inflammation reduction over macrophage cells after the treatment of nanogels. (D) Griess assay was performed to determine the anti-inflammatory performance of nanogels. (E) Hemolysis activity was evaluated using RBC cells with the treatment of nanogels. (F)-(G) Antimicrobial efficacy of nanogels was examined with two pathogens (such as S. aureus & S. epidermis).

The assay is based on the degree of the erythrolysis and hemoglobin dissociation when the nanogels are in contact with blood. For skin care applications the nanogels should as expected [81]be non-hemolytic. After the centrifugation, the upper layer of the experimental group and the negative control group are colorless and transparent liquid, and the lower layer has a thin layer of red blood cell sediment (Fig. 6E). The results indicate that nanogels do not induce hemolysis.

Antibacterial agents are an important part of modern medicine with antibiotics being the most prevalent class in spite of adverse side effects and the development of resistance [82]. Alternative are searched for with silver and gold-based nanoparticles being promising but are not ideal due to either toxicity or price not satisfactory alternatives. Antibacterial properties of naturally occurring phenolic components [83–85] inspired the investigation of the antimicrobial activity of ZC-CSNG. Potential mechanisms of action include destabilizing the cytoplasmic membrane, enhancing membrane permeability, or binding and

interacting with DNA [86]. The *in vitro* antibacterial activities of the ZC-CSNG was examined against two pathogens – *S. aureus* and *S. epidermidis* [52] – using an MIC, MBC, Live/Dead and SEM techniques (Fig. 6G, S12 and S13). MIC values against *S. aureus and S. epidermidis* were 1.5 and 0.2 mg/mL, respectively. MBC values were 1.5 and 0.4 mg/mL against S. aureus and S. epidermidis similar to the reported effect of p-CA [87]. Live and Dead staining in the concentration range 0.2 to 1.5 mg/mL ZC-CSNG indicated that the red cells (dead) are increasing with increase in concentration of ZC-CSNG, while green cells (live) are significantly reducing. Furthermore, SEM image were acquired at two concentrations (0.4 and 0.8 mg/mL; Fig. 7) and fluorescence microscopy in the full concentration range (Figure S13). The treated cells membranes become more porous with visible alterations in both the bacterial species, which indicate damage to the cell membrane. Alternative mechanism of action are possible and widely discussed [88]. Our study primarily focused on the antibacterial effects of the nanogel against Gram-positive bacteria, which are significant in wound infections due to their thick peptidoglycan layers, biofilm formation, and potent exotoxins. The nanogel, containing p-Coumaric acid, showed strong inhibitory effects on Gram-positive bacteria like Staphylococcus aureus and Staphylococcus epidermidis, underscoring its potential in treating infections where these bacteria are predominant.

While Gram-positive bacteria were the primary focus due to their impact on wound healing, we also tested the nanogel against Gram-negative bacteria (E. coli), as detailed in the Supporting Information (S14). However, no significant inhibitory effect was observed. This result aligns with the known structural differences of Gram-negative bacteria, whose outer membranes limit the penetration of p-Coumaric acid. Despite this limitation, our findings demonstrate efficacy of the nanogel where it is most needed, with future research aiming to broaden its antibacterial spectrum.

4. Conclusions

Our investigation into sprayable nanogels derived from chitosan (CS) polymers confirms our initial hypotheses, demonstrating their superiority over traditional wound dressings. The incorporation of sulfobetaine and p-coumaric acid enhances antioxidant and antibacterial properties, facilitating accelerated wound closure and reduced inflammation. These nanogels exhibit multifunctional attributes, including antifouling and anti-ROS effects, ensuring versatility in wound care management. The synthesis approach proves scalable, yielding stable (>28 days), easily sprayable nano-hydrogels with lasting efficacy. *In vitro* studies validate enhanced cell proliferation, migration, and robust antioxidant capabilities. Our findings endorse CS-based nanogels as promising, eco-friendly wound care solutions, advancing drug delivery systems for bacterial contamination.

CRediT authorship contribution statement

Suman Basak: Writing – review & editing, Writing – original draft, Visualization, Validation, Software, Resources, Project administration, Methodology, Investigation, Funding acquisition, Formal analysis, Data curation, Conceptualization. **Priyanka Singh:** Writing – review & editing, Resources, Methodology, Formal analysis, Data curation. **Arjen Weller:** Resources, Methodology, Formal analysis, Data curation. **Firoz Babu Kadumudi:** Writing – review & editing, Formal analysis, Data curation, Investigation. **Paul J. Kempen:** Resources. **Ivan Mijakovic:** Investigation. **Alireza Dolatshahi-Pirouz:** Resources, Investigation. **Kristoffer Almdal:** Writing – review & editing, Visualization, Validation, Project administration, Investigation, Funding acquisition, Conceptualization.

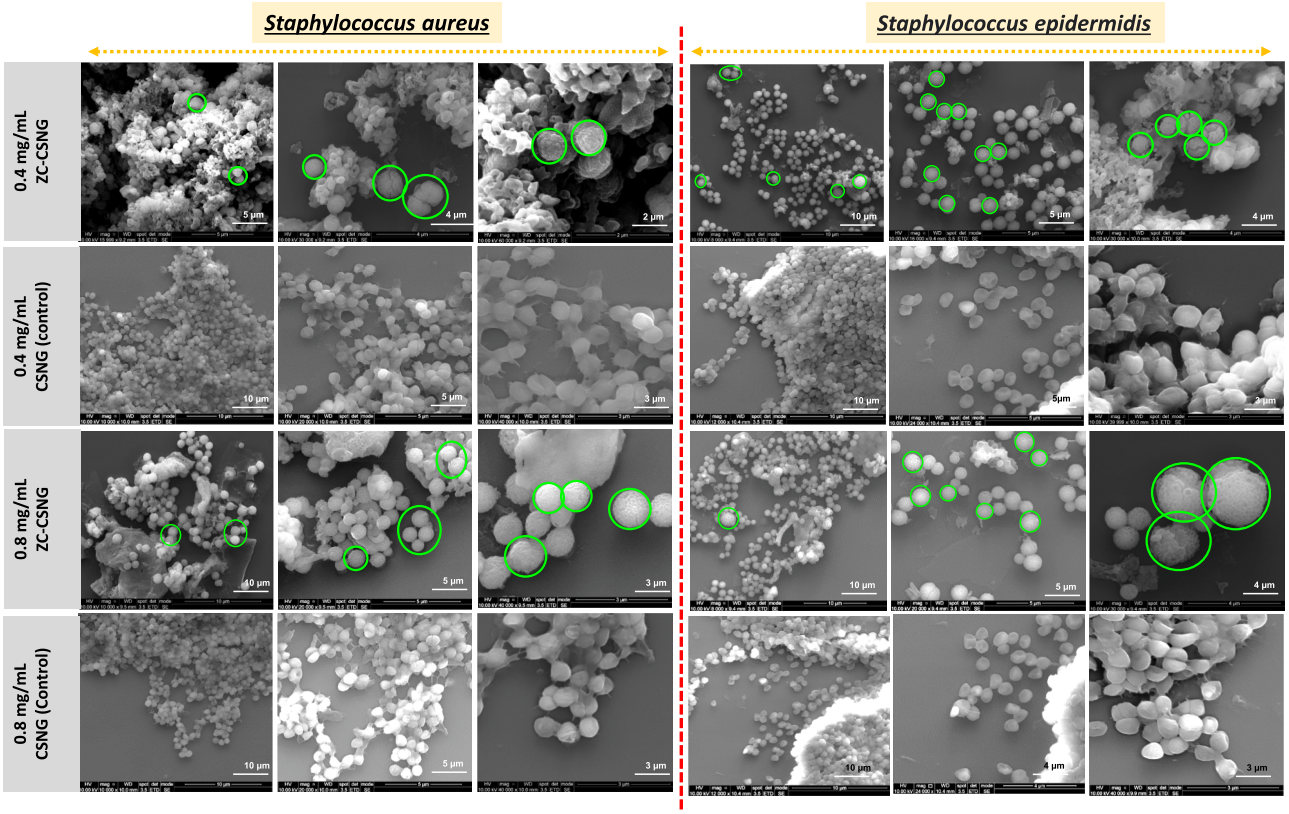

Fig. 7. Scanning electron microscopy (SEM) images of bacteria cells treated with different concentrations of nanogels, (left panel) S. aureus and (right panel) S. epidermidis. The green circle indicate the cell membrane disruption due to the p-CA nanogel effects.

Declaration of competing interest

The authors declare that they have no known competing financial interests or personal relationships that could have appeared to influence the work reported in this paper.

Acknowledgements

SB, NL and KA. Financial support from Independent Research Fund Denmark, grant 7017-00366B is kindly acknowledged.

Appendix A. Supplementary data

Supplementary data to this article can be found online at https://doi.org/10.1016/j.cej.2024.158312.

Data availability

Data will be made available on request.

References

[1] J. Frenk, Health and the economy, Harv. Int. Rev. 35 (4) (2014) 62–64.
[2] G. FrykbergRobert, Challenges in the treatment of chronic wounds, Adv. Wound Care (2015).
[3] S. Enoch, J.E. Grey, K.G. Harding, Non-surgical and drug treatments, BMJ 332 (7546) (2006) 900–903.
[4] Y. Liang, J. He, B. Guo, Functional hydrogels as wound dressing to enhance wound healing, ACS Nano 15 (8) (2021) 12687–12722.
[5] Z. Pan, H. Ye, D. Wu, Recent advances on polymeric hydrogels as wound dressings, APL Bioeng. 5 (1) (2021).
[6] J. Xiang, L. Shen, Y. Hong, Status and future scope of hydrogels in wound healing: Synthesis, materials and evaluation, Eur. Polym. J. 130 (2020) 109609.
[7] R.T. Chacko, J. Ventura, J. Zhuang, S. Thayumanavan, Polymer nanogels: a versatile nanoscopic drug delivery platform, Adv. Drug Deliv. Rev. 64 (9) (2012) 836–851.
[8] K. Raemdonck, J. Demeester, S. De Smedt, Advanced nanogel engineering for drug delivery, Soft Matter 5 (4) (2009) 707–715.
[9] H. Ayame, N. Morimoto, K. Akiyoshi, Self-assembled cationic nanogels for intracellular protein delivery, Bioconjug. Chem. 19 (4) (2008) 882–890.
[10] X. Li, Z. Ouyang, H. Li, C. Hu, P. Saha, L. Xing, A. Pich, Dendrimer-decorated nanogels: Efficient nanocarriers for biodistribution in vivo and chemotherapy of ovarian carcinoma, Bioact. Mater. 6 (10) (2021) 3244–3253.
[11] S. Bazban-Shotorbani, H.A. Khare, J. Kajtez, S. Basak, J.H. Lee, N. Kamaly, Effect of nanoparticle biophysicochemical properties on binding and transport across cardiovascular endothelial dysfunction models, ACS Appl. Nano Mater. 4 (4) (2021) 4077–4091.
[12] L. Zhang, Z. Cao, Y. Li, J.-R. Ella-Menye, T. Bai, S. Jiang, Softer zwitterionic nanogels for longer circulation and lower splenic accumulation, ACS Nano 6 (8) (2012) 6681–6686.
[13] S. Basak, I. Mukherjee, T.K. Das, Injectable biocompatible RAFT mediated nitroxide nanogels: A robust ROS-reduction antioxidant approach, Colloids Surfaces B: Biointerf. (2024) 113790.
[14] Y. Chen, N. Ballard, S.A. Bon, Waterborne polymer nanogels non-covalently crosslinked by multiple hydrogen bond arrays, Polym. Chem. 4 (2) (2013) 387–392.
[15] M. Hartlieb, D. Pretzel, M. Wagner, S. Hoeppener, P. Bellstedt, M. Görlach, U. S. Schubert, Core cross-linked nanogels based on the self-assembly of double hydrophilic poly (2-oxazoline) block copolymers, J. Mater. Chem. B 3 (9) (2015) 1748–1759.
[16] H. Wang, Q. Chen, S. Zhou, Carbon-based hybrid nanogels: A synergistic nanoplatform for combined biosensing, bioimaging, and responsive drug delivery, Chem. Soc. Rev. 47 (11) (2018) 4198–4232.
[17] K. Elkhoury, C.S. Russell, L. Sanchez-Gonzalez, A. Mostafavi, T.J. Williams, C. Kahn, A. Tamayol, Soft-nanoparticle functionalization of natural hydrogels for tissue engineering applications, Adv. Healthc. Mater. 8 (18) (2019) 1900506.
[18] Y. Fan, M. Lüchow, Y. Zhang, J. Lin, L. Fortuin, S. Mohanty, M. Malkoch, Nanogel encapsulated hydrogels as advanced wound dressings for the controlled delivery of antibiotics, Adv. Funct. Mater. 31 (7) (2021) 2006453.
[19] S. Basak, H.A. Khare, M. Roursgaard, P.J. Kempen, J.H. Lee, S. Bazban-Shotorbani, K. Almdal, Simultaneous cross-linking and cross-polymerization of enzyme responsive polyethylene glycol nanogels in confined aqueous droplets for reduction of low-density lipoprotein oxidation, Biomacromolecules 22 (2) (2020) 386–398.
[20] D. Das, A.P. Rameshbabu, P. Ghosh, P. Patra, S. Dhara, S. Pal, Biocompatible nanogel derived from functionalized dextrin for targeted delivery of doxorubicin hydrochloride to MG 63 cancer cells, Carbohydr. Polym. 171 (2017) 27–38.
[21] Y. Yin, B. Hu, X. Yuan, L. Cai, H. Gao, Q. Yang, Nanogel: A versatile nano-delivery system for biomedical applications, Pharmaceutics 12 (3) (2020) 290.
[22] N. Drude, S. Singh, O.H. Winz, M. Möller, F.M. Mottaghy, A. Morgenroth, Multistage passive and active delivery of radiolabeled nanogels for superior tumor penetration efficiency, Biomacromolecules 18 (8) (2017) 2489–2498.
[23] E. van Andel, S.C. Lange, S.P. Pujari, E.J. Tijhaar, M.M. Smulders, H.F. Savelkoul, H. Zuilhof, Systematic comparison of zwitterionic and non-zwitterionic antifouling polymer brushes on a bead-based platform, Langmuir 35 (5) (2018) 1181–1191.
[24] Y. Zhang, Y. Liu, B. Ren, D. Zhang, S. Xie, Y. Chang, J. Zheng, Fundamentals and applications of zwitterionic antifouling polymers, J. Phys. D Appl. Phys. 52 (40) (2019) 403001.
[25] Y. Chang, Y.J. Shih, C.J. Lai, H.H. Kung, S. Jiang, Blood-inert surfaces via ion-pair anchoring of zwitterionic copolymer brushes in human whole blood, Adv. Funct. Mater. 23 (9) (2013) 1100–1110.
[26] M.-C. Sin, S.-H. Chen, Y. Chang, Hemocompatibility of zwitterionic interfaces and membranes, Polym. J. 46 (8) (2014) 436–443.
[27] I. Mukherjee, A. Ghosh, P. Bhadury, P. De, Matrix assisted antibacterial activity of polymer conjugates with pendant antibiotics, and bioactive and biopassive moieties, J. Mater. Chem. B 7 (18) (2019) 3007–3018.
[28] T.K. Das, S. Basak, S. Ganguly, 2D nanomaterial for microplastic Removal: A critical review, Chem. Eng. J. 152451 (2024).
[29] T.J. Plegue, K.M. Kovach, A.J. Thompson, J.A. Potkay, Stability of polyethylene glycol and zwitterionic surface modifications in PDMS microfluidic flow chambers, Langmuir 34 (1) (2018) 492–502.
[30] S. Basak, Design, synthesis and development of biologically inspired polymeric nanomedicines for the treatment of advanced atherosclerosis, DTU Health Tech, 2019. PhD-thesis.
[31] S. Basak, N. Kamaly, Bioinspired anti-oxidising and anti-atherogenic matrix-metalloproteinase responsive polymeric nanogels. 2018 E-MRS Fall Meeting and Exhibit, 2018.
[32] X. Chen, X. Qiu, M. Hou, X. Wu, Y. Dong, Y. Ma, Y. Wei, Differences in zwitterionic sulfobetaine and carboxybetaine dextran-based hydrogels, Langmuir 35 (5) (2018) 1475–1482.
[33] B. Oktay, N. Kayaman-Apohan, M. Süleymanoğlu, S. Erdem-Kuruca, Zwitterionic phosphorylcholine grafted chitosan nanofiber: Preparation, characterization and in-vitro cell adhesion behavior, Mater. Sci. Eng. C 73 (2017) 569–578.
[34] E. Urnukhsaikhan, B.-E. Bold, A. Gunbileg, N. Sukhbaatar, T. Mishig-Ochir, Antibacterial activity and characteristics of silver nanoparticles biosynthesized from Carduus crispus, Sci. Rep. 11 (1) (2021) 21047.
[35] A.R. Gliga, S. Skoglund, I. Odnevall Wallinder, B. Fadeel, H.L. Karlsson, Size-dependent cytotoxicity of silver nanoparticles in human lung cells: the role of cellular uptake, agglomeration and Ag release, Part. Fibre Toxicol. 11 (2014) 1–17.
[36] C. Liao, Y. Li, S.C. Tjong, Bactericidal and cytotoxic properties of silver nanoparticles, Int. J. Mol. Sci. 20 (2) (2019) 449.
[37] C. Dunnill, T. Patton, J. Brennan, J. Barrett, M. Dryden, J. Cooke, N. T. Georgopoulos, Reactive oxygen species (ROS) and wound healing: the functional role of ROS and emerging ROS-modulating technologies for augmentation of the healing process, Int. Wound J. 14 (1) (2017) 89–96.
[38] K. Hensley, K.A. Robinson, S.P. Gabbita, S. Salsman, R.A. Floyd, Reactive oxygen species, cell signaling, and cell injury, Free Radic. Biol. Med. 28 (10) (2000) 1456–1462.
[39] T. Maheswary, A.A. Nurul, M.B. Fauzi, The insights of microbes' roles in wound healing: A comprehensive review, Pharmaceutics 13 (7) (2021) 981.
[40] I.M. Comino-Sanz, M.D. López-Franco, B. Castro, P.L. Pancorbo-Hidalgo, Antioxidant dressing therapy versus standard wound care in chronic wounds (the REOX study): study protocol for a randomized controlled trial, Trials 21 (2020) 1–9.
[41] I.M. Comino-Sanz, M.D. López-Franco, B. Castro, P.L. Pancorbo-Hidalgo, The role of antioxidants on wound healing: A review of the current evidence, J. Clin. Med. 10 (16) (2021) 3558.
[42] T. Dai, M. Tanaka, Y.-Y. Huang, M.R. Hamblin, Chitosan preparations for wounds and burns: antimicrobial and wound-healing effects, Expert Rev. Anti Infect. Ther. 9 (7) (2011) 857–879.
[43] Y. Shen, X. Song, L. Li, J. Sun, Y. Jaiswal, J. Huang, H. Zhang, Protective effects of p-coumaric acid against oxidant and hyperlipidemia-an in vitro and in vivo evaluation, Biomed. Pharmacother. 111 (2019) 579–587.
[44] J. Liu, H. Sun, F. Dong, Q. Xue, G. Wang, S. Qin, Z. Guo, The influence of the cation of quaternized chitosans on antioxidant activity, Carbohydr. Polym. 78 (3) (2009) 439–443.
[45] P. Deng, J. Chen, L. Yao, P. Zhang, J. Zhou, Thymine-modified chitosan with broad-spectrum antimicrobial activities for wound healing, Carbohydr. Polym. 257 (2021) 117630.
[46] P. Deng, W. Jin, Z. Liu, M. Gao, J. Zhou, Novel multifunctional adenine-modified chitosan dressings for promoting wound healing, Carbohydr. Polym. 260 (2021) 117767.
[47] M. Hasnain, T. Kanwal, K. Rehman, S.R.U. Rehman, S. Aslam, T. Roome, S. Yasmeen, Microarray needles comprised of arginine-modified chitosan/PVA hydrogel for enhanced antibacterial and wound healing potential of curcumin, Int. J. Biol. Macromol. 253 (2023) 126697.
[48] C. Sun, X. Zeng, S. Zheng, Y. Wang, Z. Li, H. Zhang, X. Yang, Bio-adhesive catechol-modified chitosan wound healing hydrogel dressings through glow discharge plasma technique, Chem. Eng. J. 427 (2022) 130843.
[49] Z. Xu, G. Liu, L. Zheng, J. Wu, A polyphenol-modified chitosan hybrid hydrogel with enhanced antimicrobial and antioxidant activities for rapid healing of diabetic wounds, Nano Res. 16 (1) (2023) 905–916.
[50] E.T.S. Damasceno, R.R. Almeida, S.Y.B. de Carvalho, G.S.G. de Carvalho, V. Mano, A.C. Pereira, L.G. de Lima Guimaraes, Lippia origanoides Kunth. essential oil

loaded in nanogel based on the chitosan and ρ-coumaric acid: Encapsulation efficiency and antioxidant activity, Ind. Crop. Prod. 125 (2018) 85–94.
[51] R. Varma, S. Vasudevan, Extraction, characterization, and antimicrobial activity of chitosan from horse mussel modiolus modiolus, ACS Omega 5 (32) (2020) 20224–20230.
[52] G.C.M. Almeida, M.M. dos Santos, N.G.M. Lima, T.A. Cidral, M.C.N. Melo, K. C. Lima, Prevalence and factors associated with wound colonization by Staphylococcus spp. and Staphylococcus aureusin hospitalized patients in inland northeastern Brazil: a cross-sectional study, BMC Infect. Dis. 14 (1) (2014) 1–8.
[53] M. Ioelovich, Crystallinity and hydrophility of chitin and chitosan, J. Chem 3 (3) (2014) 7–14.
[54] S. Xiao, X. He, Z. Zhao, G. Huang, Z. Yan, Z. He, J. Yang, Strong anti-polyelectrolyte zwitterionic hydrogels with superior self-recovery, tunable surface friction, conductivity, and antifreezing properties, Eur. Polym. J. 148 (2021) 110350.
[55] B.K. Wilson, R.K. Prud'homme, Nanoparticle size distribution quantification from transmission electron microscopy (TEM) of ruthenium tetroxide stained polymeric nanoparticles, J. Colloid Interface Sci. 604 (2021) 208–220.
[56] K.B. Pandey, S.I. Rizvi, Plant polyphenols as dietary antioxidants in human health and disease, Oxid. Med. Cell. Longev. 2 (2009) 270–278.
[57] D.M. Pereira, P. Valentão, J.A. Pereira, P.B. Andrade, Phenolics: from Chemistry to Biology Vol. 14 (2009) 2202–2211.
[58] S. Basak, H.A. Khare, P.J. Kempen, N. Kamaly, K. Almdal, Nanoconfined anti-oxidizing RAFT nitroxide radical polymer for reduction of low-density lipoprotein oxidation and foam cell formation, Nanoscale Adv. 4 (3) (2022) 742–753.
[59] J. Chen, J. Yang, L. Ma, J. Li, N. Shahzad, C.K. Kim, Structure-antioxidant activity relationship of methoxy, phenolic hydroxyl, and carboxylic acid groups of phenolic acids, Sci. Rep. 10 (1) (2020) 2611.
[60] Y.-J. Shang, B.-Y. Liu, M.-M. Zhao, Details of the Antioxidant Mechanism of Hydroxycinnamic Acids, Czech J. Food Sci. 33 (3) (2015).
[61] O. Taofiq, A.M. González-Paramás, M.F. Barreiro, I.C. Ferreira, Hydroxycinnamic acids and their derivatives: Cosmeceutical significance, challenges and future perspectives, a review, Molecules 22 (2) (2017) 281.
[62] Antonis Zampelas, R. M. (2015). *Antioxidants in Health and Disease*. (1st Edition ed.).
[63] F. Avelelas, A. Horta, L.F. Pinto, S. Cotrim Marques, P. Marques Nunes, R. Pedrosa, S.M. Leandro, Antifungal and antioxidant properties of chitosan polymers obtained from nontraditional Polybius henslowii sources, Mar. Drugs 17 (4) (2019) 239.
[64] P. Eslami, F. Rossi, S. Fedeli, Hybrid nanogels: stealth and biocompatible structures for drug delivery applications, Pharmaceutics 11 (2) (2019) 71.
[65] I.A. Darby, B. Laverdet, F. Bonté, A. Desmoulière, Fibroblasts and myofibroblasts in wound healing, Clin. Cosmet. Investig. Dermatol. (2014) 301–311.
[66] L.E. Tracy, R.A. Minasian, E. Caterson, Extracellular matrix and dermal fibroblast function in the healing wound, Adv. Wound Care 5 (3) (2016) 119–136.
[67] Y. Oishi, I. Manabe, Macrophages in inflammation, repair and regeneration, Int. Immunol. 30 (11) (2018) 511–528.
[68] Y. Tang, X. Cai, Y. Xiang, Y. Zhao, X. Zhang, Z. Wu, Cross-linked antifouling polysaccharide hydrogel coating as extracellular matrix mimics for wound healing, J. Mater. Chem. B 5 (16) (2017) 2989–2999.
[69] S. Xiao, B. Ren, L. Huang, M. Shen, Y. Zhang, M. Zhong, J. Zheng, Salt-responsive zwitterionic polymer brushes with anti-polyelectrolyte property, Curr. Opin. Chem. Eng. 19 (2018) 86–93.
[70] H. Latifi-Pupovci, Z. Kuçi, S. Wehner, H. Bönig, R. Lieberz, T. Klingebiel, S. Kuçi, In vitro migration and proliferation ("wound healing") potential of mesenchymal stromal cells generated from human CD271+ bone marrow mononuclear cells, J. Transl. Med. 13 (2015) 1–9.
[71] R. Pan, G. Liu, Y. Zeng, X. He, Z. Ma, Y. Wei, L. Tao, A multi-responsive self-healing hydrogel for controlled release of curcumin, Polym. Chem. 12 (16) (2021) 2457–2463.
[72] K.E. Johnson, T.A. Wilgus, Vascular endothelial growth factor and angiogenesis in the regulation of cutaneous wound repair, Adv. Wound Care 3 (10) (2014) 647–661.
[73] M.P. Rodero, F. Licata, L. Poupel, P. Hamon, K. Khosrotehrani, C. Combadiere, A. Boissonnas, In vivo imaging reveals a pioneer wave of monocyte recruitment into mouse skin wounds, PLoS One 9 (10) (2014) e108212.
[74] M.G. Tonnesen, X. Feng, R.A. Clark, Angiogenesis in Wound Healing Vol. 5 (2000) 40–46.
[75] K. Popko, E. Gorska, A. Stelmaszczyk-Emmel, R. Plywaczewski, A. Stoklosa, D. Gorecka, U. Demkow, Proinflammatory cytokines Il-6 and TNF-α and the development of inflammation in obese subjects, Eur. J. Med. Res. 15 (2010) 1–3.
[76] H. Zhu, Q.-H. Liang, X.-G. Xiong, Y. Wang, Z.-H. Zhang, M.-J. Sun, D. Wu, Anti-inflammatory effects of p-coumaric acid, a natural compound of Oldenlandia diffusa, on arthritis model rats, Evid.-Based Complement. Alternat. Med. 2018 (2018).
[77] S.B. Abramson, Nitric oxide in inflammation and pain associated with osteoarthritis, Arthritis Res. Ther. 10 (2) (2008) 1–7.
[78] C.-Y. Lin, W.-H. Wang, S.-H. Chen, Y.-W. Chang, L.-C. Hung, C.-Y. Chen, Y.-H. Chen, Lipopolysaccharide-induced nitric oxide, prostaglandin E2, and cytokine production of mouse and human macrophages are suppressed by pheophytin-b, Int. J. Mol. Sci. 18 (12) (2017) 2637.
[79] A.A. Qureshi, X.Q. Guan, J.C. Reis, C.J. Papasian, S. Jabre, D.C. Morrison, N. Qureshi, Inhibition of nitric oxide and inflammatory cytokines in LPS-stimulated murine macrophages by resveratrol, a potent proteasome inhibitor, Lipids Health Dis. 11 (1) (2012) 1–17.
[80] Y. Zhao, J. Liu, C. Liu, X. Zeng, X. Li, J. Zhao, Anti-inflammatory effects of p-coumaric acid in LPS-stimulated RAW264. 7 cells: Involvement of NF-κB and MAPKs pathways, Med. Chem 6 (2016) 327–330.
[81] X. Jin, J. Yuan, J. Shen, Zwitterionic polymer brushes via dopamine-initiated ATRP from PET sheets for improving hemocompatible and antifouling properties, Colloids Surf. B Biointerfaces 145 (2016) 275–284.
[82] B. Li, T.J. Webster, Bacteria antibiotic resistance: New challenges and opportunities for implant-associated orthopedic infections, J. Orthop. Res.® 36 (1) (2018) 22–32.
[83] S. Macé, L.T. Hansen, H.V. Rupasinghe, Anti-bacterial activity of phenolic compounds against Streptococcus pyogenes, Medicines 4 (2) (2017) 25.
[84] M.R. Vaquero, M.R. Alberto, M.M. De Nadra, Antibacterial effect of phenolic compounds from different wines, Food Control 18 (2) (2007) 93–101.
[85] X. Zhu, H. Zhang, R. Lo, Phenolic compounds from the leaf extract of artichoke (Cynara scolymus L.) and their antimicrobial activities, J. Agric. Food Chem. 52 (24) (2004) 7272–7278.
[86] M. Contardi, A. Alfaro-Pulido, P. Picone, S. Guzman-Puyol, L. Goldoni, J.J. Benítez, G. Cusimano, Low molecular weight ε-caprolactone-p-coumaric acid copolymers as potential biomaterials for skin regeneration applications, PLoS One 14 (4) (2019) e0214956.
[87] M. Contardi, J.A. Heredia-Guerrero, S. Guzman-Puyol, M. Summa, J.J. Benítez, L. Goldoni, M. Di Carlo, Combining dietary phenolic antioxidants with polyvinylpyrrolidone: Transparent biopolymer films based on p-coumaric acid for controlled release, J. Mater. Chem. B 7 (9) (2019) 1384–1396.
[88] L.-L. Zhang, L.-F. Zhang, J.-G. Xu, Chemical composition, antibacterial activity and action mechanism of different extracts from hawthorn (Crataegus pinnatifida Bge.), Sci. Rep. 10 (1) (2020) 8876.